

# Predicting electron spin decoherence with a many-body first-principles approach

Jinsoo Park,<sup>1</sup> Jin-Jian Zhou,<sup>2</sup> and Marco Bernardi<sup>1,\*</sup>

<sup>1</sup>*Department of Applied Physics and Materials Science,  
California Institute of Technology, Pasadena, CA 91125, USA.*

<sup>2</sup>*School of Physics, Beijing Institute of Technology, Beijing 100081, China.*

Developing a microscopic understanding of spin decoherence is essential to advancing quantum technologies<sup>1-4</sup>. Electron spin decoherence due to atomic vibrations (phonons) plays a special role as it sets an intrinsic limit to the performance of spin-based quantum devices. Two main sources of phonon-induced spin decoherence – the Elliott-Yafet (EY) and Dyakonov-Perel (DP) mechanisms – have distinct physical origins and theoretical treatments<sup>5-7</sup>. Here we show calculations that unify their modeling and enable accurate predictions of spin relaxation and precession in semiconductors. We compute the phonon-dressed vertex of the spin-spin correlation function, with a treatment analogous to the calculation of the anomalous electron magnetic moment in QED<sup>8</sup>. We find that the vertex correction provides a giant renormalization of the electron spin dynamics in solids, greater by many orders of magnitude than the corresponding correction in vacuum. Our work demonstrates a general approach for quantitative analysis of spin decoherence in materials, advancing the quest for spin-based quantum technologies.

Spin decoherence from phonons is a pressing question in quantum technology – it governs spin transport<sup>9-14</sup> and limits the manipulation of quantum information<sup>1-4,15-17</sup> and the realization of reliable quantum devices<sup>18-20</sup>. Previous work has identified two key sources of phonon-induced spin decoherence in the presence of spin-orbit coupling (SOC) – the Elliott-Yafet (EY) mechanism<sup>5,6</sup>, whereby electron-phonon (*e-ph*) collisions change the spin direction, and the Dyakonov-Perel (DP) mechanism<sup>7</sup> originating from spin precession between *e-ph* collisions. Historically, these two mechanisms have been described with distinct theoretical models<sup>5-7,21,22</sup>, although significant efforts have been made to unify them, for example using real-time evolution of spin ensembles<sup>23-25</sup> or analyzing quasiparticle broadening in model systems<sup>26-28</sup>.

However, formulating a theory that encompasses both the EY and DP mechanisms, and developing corresponding quantitative calculations of spin decoherence in real materials, are still outstanding challenges. Many-body approaches combined with density functional theory (DFT) and related first-principles calculations are particularly promising to tackle this problem. These *ab initio* methods have become a gold standard for calculations of *e-ph* interactions and transport phenomena in solids<sup>29-39</sup>. Recent work has extended this framework to compute spin-flip processes due to *e-ph* interactions, leading to predictions of EY spin decoherence within the spin relaxation time approximation (sRTA)<sup>40</sup>. It is widely accepted that the sRTA neglects spin precession, and thus a different formalism is needed to capture the DP mechanism<sup>21,25</sup>.

Inspired by the work of Kim et al.<sup>41</sup>, which rigorously proved that the Boltzmann equation is equivalent to the ladder vertex correction to the conductivity, we ask if a similar many-body approach can be used to

study the spin susceptibility and spin dynamics. The development of this framework, and of corresponding first-principles calculations, would provide a viable tool to study phonon-induced spin decoherence, mimicking the progress of first-principles studies of charge transport<sup>29-39</sup>. These accurate predictions of spin decoherence would advance both condensed matter theory and spin-based quantum technology.

Here we present a many-body theory of spin relaxation and develop precise *ab initio* calculations of phonon-induced spin decoherence in semiconductors. Our approach calculates the *e-ph* vertex corrections to the spin susceptibility, with an accurate account of electronic and vibrational states, SOC, and *e-ph* interactions. We compute the spin relaxation times (SRTs) of electron and hole carriers in Si and GaAs – two key candidates for spin-based quantum computing – and in a 2D semiconductor with strong SOC, WSe<sub>2</sub>. Our predicted SRTs are in excellent agreement with experiments over a wide temperature range. We demonstrate that our formalism can calculate both spin relaxation and spin precession, and capture EY and DP decoherence on equal footing; we contrast these results with the sRTA, which lacks DP decoherence and gives unphysical SRTs near the band gap. Our analysis shows that the *e-ph* interactions lead to a colossal renormalization of the electron spin dynamics in solids, significantly modifying the SRTs and spin precession rates (SPRs). The theoretical and computational method developed in this work paves the way for a deeper understanding of electron spin decoherence, with broad implications for quantum materials and devices.

To describe phonon-induced spin decoherence, we consider the Kubo formula for the spin-spin correlation function<sup>42</sup>, and include the ladder vertex correction<sup>41</sup> from *e-ph* interactions (see Fig. 1a). We derive a Bethe-Salpeter equation for the phonon-dressed spin vertex (in short, spin-phonon BSE), represented diagrammatically

---

\* Corresponding author: [bmarco@caltech.edu](mailto:bmarco@caltech.edu)

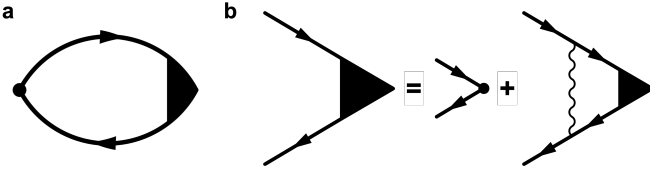


FIG. 1. **Feynman diagrams for spin decoherence.** **a** Bubble diagram for the spin-spin correlation function including the vertex correction. **b** Bethe-Salpeter equation for the phonon-dressed spin vertex in the ladder approximation.

in Fig. 1b, which we write as (see Methods):

$$\mathbf{s}\Lambda_{\mathbf{k}}(\varepsilon) = \mathbf{s}\mathbf{k} + \frac{1}{V} \sum_{\nu\mathbf{q}\pm} \mathbf{g}_{\nu\mathbf{k}\mathbf{q}}^{\dagger} \left[ \mathbf{G}^A \mathbf{s} \Lambda \mathbf{G}^R \right]_{\varepsilon \pm \omega_{\nu\mathbf{q}}} \mathbf{g}_{\nu\mathbf{k}\mathbf{q}} F_{\pm}(T) \quad (1)$$

where all bolded quantities are matrices in Bloch basis. Above,  $\mathbf{s}\Lambda_{\mathbf{k}}(\varepsilon) = \mathbf{s}_{nn'\mathbf{k}} \Lambda_{nn'\mathbf{k}}(\varepsilon)$  is the phonon-dressed spin vertex,  $\Lambda_{nn'\mathbf{k}}^{\alpha}(\varepsilon)$  is the vertex correction at energy  $\varepsilon$  for the Cartesian direction  $\alpha$ , and  $\mathbf{s}_{nn'\mathbf{k}} = \langle n\mathbf{k} | \frac{\hbar}{2} \hat{\sigma} | n'\mathbf{k} \rangle$  is the bare spin vertex;  $\mathbf{G}^{R/A}$  are the retarded/advanced interacting Green's functions<sup>42</sup>,  $V$  is the system volume,  $F_{\pm}(T)$  is a phonon occupation factor at temperature  $T$ , and  $[\mathbf{g}_{\nu\mathbf{k}\mathbf{q}}]_{nm} = g_{nm\nu}(\mathbf{k}, \mathbf{q})$  are  $e$ -ph matrix elements<sup>30</sup>.

The vertex correction  $\Lambda$  governs the spin dynamics by renormalizing the microscopic SRTs and SPRs (see Methods). The macroscopic SRTs are obtained as the thermal average

$$\tau_{\alpha\beta}^{(s)} = \frac{\sum_{n\mathbf{k}} s_{nn\mathbf{k}}^{\alpha} s_{nn\mathbf{k}}^{\beta} \tau_{n\mathbf{k}}^{\text{e-ph}} \Lambda_{nn\mathbf{k}}^{\beta}(\varepsilon_{n\mathbf{k}}) \left(-\frac{df_{n\mathbf{k}}}{d\varepsilon}\right)}{\sum_{n\mathbf{k}} s_{nn\mathbf{k}}^{\alpha} s_{nn\mathbf{k}}^{\beta} \left(-\frac{df_{n\mathbf{k}}}{d\varepsilon}\right)}, \quad (2)$$

where  $\tau_{n\mathbf{k}}^{\text{e-ph}}$  are  $e$ -ph collision times<sup>29,42</sup>. For  $\alpha = \beta$ , Eq. (2) gives the longitudinal SRT, usually called  $T_1$ , along the direction  $\alpha$ , while for  $\alpha \neq \beta$  one obtains the transverse SRT,  $T_2$  (not computed here)<sup>43</sup>. The renormalized microscopic SRTs ( $\tau_{nn'\mathbf{k}}^{\alpha}$ ) and SPRs ( $\omega_{nn'\mathbf{k}}^{\alpha}$ ), which are matrices in Bloch basis, are computed from the vertex correction using

$$\frac{1}{\tau_{nn'\mathbf{k}}^{\alpha}(\varepsilon) + i\omega_{nn'\mathbf{k}}^{\alpha}(\varepsilon)} \equiv \frac{\Lambda_{nn'\mathbf{k}}^{\alpha}(\varepsilon)}{i(\Sigma_{n\mathbf{k}}^R - \Sigma_{n'\mathbf{k}}^A) + i(\varepsilon_{n\mathbf{k}} - \varepsilon_{n'\mathbf{k}})}, \quad (3)$$

with  $\Sigma^{A/R}$  the advanced/retarded  $e$ -ph self-energy<sup>29</sup>. The diagonal components with  $n = n'$  give the renormalized microscopic SRTs,  $\tau_{n\mathbf{k}}^{\beta} = \tau_{n\mathbf{k}}^{\text{e-ph}} \Lambda_{nn\mathbf{k}}^{\beta}(\varepsilon_{n\mathbf{k}})$  entering Eq. (2), and the renormalized SPRs,  $\omega_{nn\mathbf{k}}^{\alpha}$ . We implement and solve Eqs. (1)-(3) in our PERTURBO code<sup>30</sup> (see Methods).

Using this formalism, in Fig. 2 we compute the *macroscopic* SRTs in Eq. (2) as a function of temperature for Si, GaAs, and monolayer WSe<sub>2</sub> (see Methods). In Si, a centrosymmetric material where spin decoherence is governed by the EY mechanism, the results are in excellent agreement with experiments<sup>13,44,45</sup> in the 100–300 K

temperature range. For example, the SRT computed at 300 K is 6.1 ns, in remarkable agreement with the 6.0 ns value measured in Ref.<sup>45</sup>. Due to the dominant EY mechanism, in this case the sRTA, which neglects spin precession, also gives accurate SRTs.

In GaAs, the SOC splits the conduction band, so spin relaxation is dominated by the DP mechanism<sup>22</sup>. Figure 2b shows our calculated SRTs for electrons in GaAs as function of temperature; the excellent agreement with experiments<sup>46–50</sup> is a strong evidence that the spin-phonon BSE describes correctly the DP mechanism. By contrast, the sRTA, which captures only the EY mechanism, clearly fails in GaAs, predicting SRTs an order of magnitude greater than experiments.

Our spin-phonon BSE achieves a similar accuracy for calculations on hole carriers. In Fig. 2c, we compute the SRTs for hole spins in monolayer WSe<sub>2</sub>, obtaining excellent agreement with all available experimental results between 20–90 K<sup>51–54</sup>. Note that the valence band of WSe<sub>2</sub> has a large ( $\sim 0.4$  eV) splitting due to SOC, leading to a precession rate far greater than the hole  $e$ -ph collision rates; in this strong precession regime, the spin dynamics is controlled by the diagonal part of the spin vertex and the DP mechanism becomes irrelevant, so EY spin decoherence dominates the SRTs. Conversely, for heavy holes in GaAs (see Fig. 2d) both EY and DP spin decoherence are important. The agreement with experiment is noteworthy in this regime where both mechanisms are relevant: our computed SRT for holes in GaAs 300 K is 200 fs, versus a 110 fs value measured by Hilton et al.<sup>55</sup>.

A key distinction between the EY and DP mechanisms is their dependence on the  $e$ -ph collision time,  $\tau_{n\mathbf{k}}^{\text{e-ph}}$  in Eq. (2): the SRT is proportional to  $\tau_{n\mathbf{k}}^{\text{e-ph}}$  for EY, and inversely proportional to  $\tau_{n\mathbf{k}}^{\text{e-ph}}$  for DP. Our spin-phonon BSE can capture both of these trends, as we show in Fig. 2e by artificially increasing  $\tau_{n\mathbf{k}}^{\text{e-ph}}$  (via the  $e$ -ph coupling strength  $|g|^2$ ) and recomputing the SRTs at 300 K for all four cases. In Si and WSe<sub>2</sub>, where EY spin decoherence is dominant, we find that at each given temperature the recomputed SRTs are directly proportional to the  $e$ -ph collision time, consistent with the EY mechanism<sup>5,6</sup>. Conversely, for electron spins in GaAs, the recomputed SRTs are inversely proportional to the  $e$ -ph collision time (see Fig. 2e), in agreement with the DP mechanism<sup>7</sup>. Note that the computed trend deviates from the conventional inverse proportionality for the DP SRTs, mainly because EY decoherence, although weak, is also present. For hole spins in GaAs, the recomputed SRTs exhibit a trend intermediate between pure EY and DP, further supporting our conclusion that both mechanisms are important for hole spins in GaAs<sup>25,56</sup>.

Spin precession in the DP mechanism is induced by the Dresselhaus SOC field, which is proportional to the band splitting for each electronic state. To examine the role of DP spin decoherence, we artificially vary the SOC band splitting and for each new value we recompute the SRTs (see Fig. 2f). For WSe<sub>2</sub>, varying the SOC band splitting

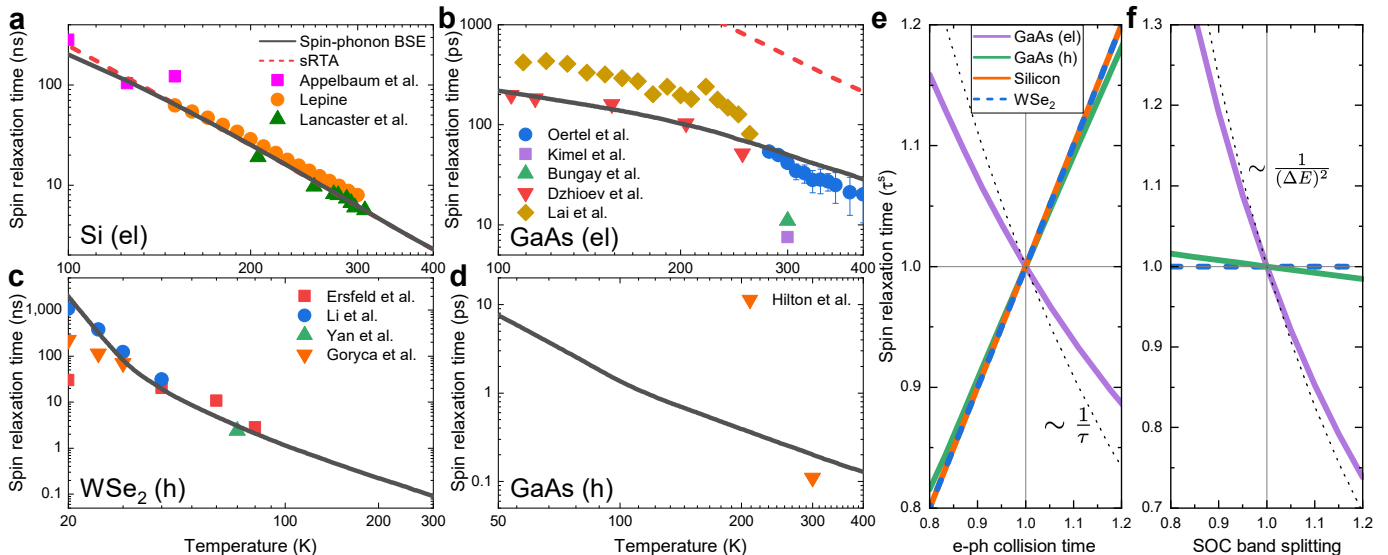


FIG. 2. **Spin relaxation times.** **a-d** Computed spin relaxation times as a function of temperature, for **a** electrons in Si, **b** electrons in GaAs, **c** holes in monolayer WSe<sub>2</sub>, and **d** holes in GaAs. Results obtained from the spin-phonon BSE (black solid line) are compared with sRTA calculations (red dashed line). Experimental results from Refs. <sup>13,44–54</sup> are shown for comparison. **e-f** The SRTs at room temperature for these four cases are recomputed by artificially increasing **e** the *e*-ph collision time and **f** the SOC band splitting entering the spin-phonon BSE. In all cases, the values of the *x*- and *y*-axes are referenced to the real systems. The conventional DP spin relaxation trend (black dotted line) is also shown for comparison.

has no effect on the SRTs, showing that spin decoherence is controlled by the EY mechanism. For electrons in GaAs, the SRTs are highly sensitive to the SOC splitting, a clear evidence that our formalism can capture the dominant DP mechanism. This dependence is weaker than in the conventional trend for pure DP,  $\tau^s \propto 1/(\Delta E)^2$ , due to the coexistence of EY decoherence. For hole carriers in GaAs, the SRTs are less sensitive to the SOC splitting than for electrons, as the decoherence originates from a balanced combination of both EY and DP mechanisms. This analysis also shows that an accurate fully-relativistic band structure is essential to describe spin precession and DP decoherence.

The phonon-induced renormalization greatly modifies the microscopic spin dynamics. Figure 3a compares sRTA and spin-phonon BSE calculations of the *microscopic* electron SRTs,  $\tau_{n\mathbf{k}}^{(s)} = \Lambda_{nn\mathbf{k}} \tau_{n\mathbf{k}}^{\text{e-ph}}$  defined below Eq. (3), in Si at 300 K for energies near the conduction band minimum. The sRTA results are strongly energy dependent, with an unphysical divergence at low energy. By contrast, the results from the spin-phonon BSE are nearly energy independent. The vertex correction makes spins with similar energy relax on the same time scale – a constant value of 6.1 ns nearly equal to the macroscopic SRT – and overcomes the limitations of the sRTA. A closer examination of the SRTs from the spin-phonon BSE (see Fig. 3b) reveals an oscillating pattern with a period equal to the  $\omega_O \approx 60$  meV energy of an optical phonon with strong *e*-ph coupling; this pattern disappears when optical phonons are neglected. This oscillation is a manifestation of the self-consistency

of the spin-phonon BSE and its ability to capture strong coupling effects beyond lowest-order perturbation theory. The same energy dependence and SRT oscillation via optical phonons are also observed for hole spins in WSe<sub>2</sub>.

Figure 3c shows the computed vertex correction  $\Lambda_{nn\mathbf{k}}^z(\varepsilon_{n\mathbf{k}})$  as a function of energy in Si. The vertex correction from *e*-ph interactions is enormous – of order  $10^5$ , and thus eight orders of magnitude greater than the vertex correction due to photons in vacuum derived by Schwinger<sup>8</sup>. We find large values ( $10^2 - 10^5$ ) for the vertex correction also in GaAs and WSe<sub>2</sub>. These colossal values account for the large differences between *e*-ph collision times (femtoseconds) and SRTs (nanoseconds) in condensed matter, and are key to accurately predicting long spin coherence times of interest in quantum technologies. The energy dependence of the vertex correction is nearly identical to that of the inverse *e*-ph collision times, thus explaining the origin of the constant trend with energy of the SRTs.

In GaAs, due to the Dresselhaus SOC band splitting, the bare spin vertex  $s_{nn'\mathbf{k}}$  acquires large off-diagonal ( $n \neq n'$ ) components that precess in the effective SOC magnetic field (with a bare SPR of  $\varepsilon_{n\mathbf{k}} - \varepsilon_{n'\mathbf{k}}$ ). While the macroscopic SRTs in Eq. (2) are determined only by the band diagonal components  $s_{nn\mathbf{k}}$ , the spin-phonon BSE couples the diagonal and off-diagonal components via Eq. (1), so spin precession modifies the SRTs.

The microscopic SRTs for electrons in GaAs (see Fig. 3d) exhibit trends similar to Si – the renormalized SRTs are nearly energy independent near the band edge, in contrast with the rapidly varying SRTs predicted by

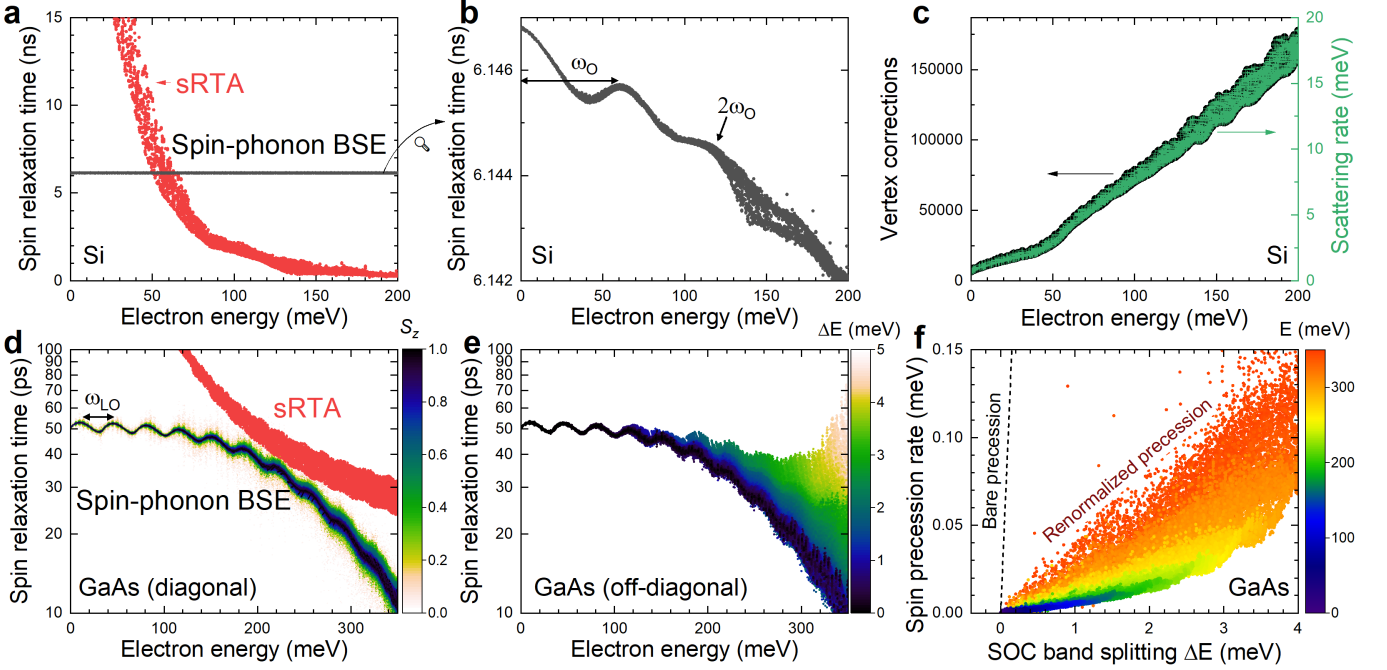


FIG. 3. **Microscopic view of spin decoherence.** **a** Microscopic electron SRTs in Si as a function of conduction band energy, computed with the spin-phonon BSE (black) and sRTA (red). **b** Zoom-in of the spin-phonon BSE results in **a**. **c** Vertex corrections  $\Lambda_{nn\mathbf{k}}$  in Si (black dots) compared with the inverse  $e$ -ph collision times (green crosses). **d** Microscopic electron SRTs in GaAs from the spin-phonon BSE, shown as a function of conduction band energy and overlaid with a color map of the expectation value of  $S_z$  for each electronic state; the sRTA results (red) are given for comparison. **e** Microscopic off-diagonal SRTs,  $\tau_{nn'\mathbf{k}}$  in Eq. (3), overlaid with a color map of the SOC band splitting  $\Delta E$ . **f** Renormalized electron SPRs in GaAs,  $\omega_{nn\mathbf{k}}$  in Eq. (3), as a function of SOC band splitting and overlaid with a color map of the conduction band energy; the bare electron SPRs (black dashed line) are given for comparison. All results are computed at 300 K. The zero of the energy axis is the conduction band minimum.

the sRTA; an oscillating pattern is evident with period equal to the 30 meV longitudinal optical (LO) phonon energy, a signature of strong coupling with LO phonons<sup>39</sup>. Yet, due to the spin precession, we also observe unique trends not found in Si. The SRTs decrease at higher energies due to the increasing spin precession (the SOC band splitting increases with energy), a manifestation of DP spin decoherence. In addition, the SRTs are strongly state dependent, as states with a smaller spin component along the quantization axis, shown with lighter colors in Fig. 3d, are subject to stronger precession.

The relaxation of the off-diagonal spin components, quantified by the off-diagonal SRTs  $\tau_{nn'\mathbf{k}}$  in Eq. (3), reveals additional signatures of the DP mechanism. Figure 3e shows these off-diagonal electron SRTs for GaAs and highlights their correlation with the SOC band splitting. When the band splitting is small (black), precession is negligible and the SRTs are identical to the diagonal SRTs in Fig. 3d. However, for increasing values of the band splitting (lighter colors), spin precession significantly enhances the SRTs. These intriguing microscopic phenomena are encoded in the vertex correction  $\Lambda$  in Eq. (3), which decreases the real part  $1/\tau_{nn'\mathbf{k}}$  of the denominator, thus slowing down spin relaxation. Similarly, the vertex correction significantly slows down spin

precession, as shown in Fig. 3f for GaAs. Bare spins precessing at a rate of 1 meV drop to a  $\sim 10^{-2}$  meV precession rate after renormalization due to phonons. These renormalized SPRs are strongly energy dependent, with higher electron energies leading to faster precession for spins with equal bare SPRs.

In conclusion, our findings highlight the dramatic effects of phonon-induced renormalization on electron spins in solids. Our spin-phonon BSE can capture renormalized spin dynamics beyond relaxation, shedding light on the interplay between the EY and DP spin decoherence mechanisms, and describing their rich physics on the same footing. This formalism reveals that the microscopic origin of the long spin coherence times in condensed matter is the colossal vertex correction from  $e$ -ph interactions. The accuracy of this framework enables precise predictions of spin decoherence in spin-based quantum technologies and advances microscopic understanding of spin dynamics in solids.

#### ACKNOWLEDGMENTS

J.P. thanks Yao Luo for fruitful discussions. This work was supported by the National Science Foundation under Grants No. DMR-1750613 and QII-TAQS 1936350.

- 1 Veldhorst, M. *et al.* A two-qubit logic gate in silicon. *Nature* **526**, 410–414 (2015).
- 2 Noiri, A. *et al.* Fast universal quantum gate above the fault-tolerance threshold in silicon. *Nature* **601**, 338–342 (2022).
- 3 Xue, X. *et al.* Quantum logic with spin qubits crossing the surface code threshold. *Nature* **601**, 343–347 (2022).
- 4 Petit, L. *et al.* Universal quantum logic in hot silicon qubits. *Nature* **580**, 355–359 (2020).
- 5 Elliott, R. J. Theory of the Effect of Spin-Orbit Coupling on Magnetic Resonance in Some Semiconductors. *Phys. Rev.* **96**, 266–279 (1954).
- 6 Yafet, Y. G Factors and Spin-Lattice Relaxation of Conduction Electrons. In Seitz, F. & Turnbull, D. (eds.) *Solid State Physics*, vol. 14, 1–98 (Academic Press, 1963).
- 7 Dyakonov, M. & Perel, V. Spin relaxation of conduction electrons in noncentrosymmetric semiconductors. *Sov. Phys. Solid State USSR* **13**, 3023–3026 (1972).
- 8 Schwinger, J. On Quantum-Electrodynamics and the Magnetic Moment of the Electron. *Phys. Rev.* **73**, 416–417 (1948).
- 9 Balasubramanian, G. *et al.* Nanoscale imaging magnetometry with diamond spins under ambient conditions. *Nature* **455**, 648–651 (2008).
- 10 Jansen, R. Silicon spintronics. *Nat. Mater.* **11**, 400–408 (2012).
- 11 Žutić, I., Fabian, J. & Das Sarma, S. Spintronics: Fundamentals and applications. *Rev. Mod. Phys.* **76**, 323–410 (2004).
- 12 Han, W., Kawakami, R. K., Gmitra, M. & Fabian, J. Graphene spintronics. *Nat. Nanotechnol.* **9**, 794–807 (2014).
- 13 Appelbaum, I., Huang, B. & Monsma, D. J. Electronic measurement and control of spin transport in silicon. *Nature* **447**, 295–298 (2007).
- 14 Železný, J., Wadley, P., Olejník, K., Hoffmann, A. & Ohno, H. Spin transport and spin torque in antiferromagnetic devices. *Nat. Phys.* **14**, 220–228 (2018).
- 15 Mi, X. *et al.* A coherent spin–photon interface in silicon. *Nature* **555**, 599–603 (2018).
- 16 Watson, T. F. *et al.* A programmable two-qubit quantum processor in silicon. *Nature* **555**, 633–637 (2018).
- 17 Wolfowicz, G. *et al.* Quantum guidelines for solid-state spin defects. *Nat. Rev. Mater.* **6**, 906–925 (2021).
- 18 Degen, C. L., Reinhard, F. & Cappellaro, P. Quantum sensing. *Rev. Mod. Phys.* **89**, 035002 (2017).
- 19 Vasyukov, D. *et al.* A scanning superconducting quantum interference device with single electron spin sensitivity. *Nat. Nanotechnol.* **8**, 639–644 (2013).
- 20 Barry, J. F. *et al.* Sensitivity optimization for NV-diamond magnetometry. *Rev. Mod. Phys.* **92**, 015004 (2020).
- 21 Baral, A., Vollmar, S., Kaltenborn, S. & Schneider, H. C. Re-examination of the Elliott–Yafet spin-relaxation mechanism. *New J. Phys.* **18**, 023012 (2016).
- 22 Mower, M. D., Vignale, G. & Tokatly, I. V. Dyakonov-Perel spin relaxation for degenerate electrons in the electron-hole liquid. *Phys. Rev. B* **83**, 155205 (2011).
- 23 Wu, M. W., Jiang, J. H. & Weng, M. Q. Spin dynamics in semiconductors. *Phys. Rep.* **493**, 61–236 (2010).
- 24 Xu, J., Habib, A., Sundararaman, R. & Ping, Y. Ab initio ultrafast spin dynamics in solids. *Phys. Rev. B* **104**, 184418 (2021).
- 25 Shen, K. & Wu, M. W. Hole spin relaxation in intrinsic and *p*-type bulk GaAs. *Phys. Rev. B* **82**, 115205 (2010).
- 26 Simon, F. *et al.* Generalized Elliott-Yafet Theory of Electron Spin Relaxation in Metals: Origin of the Anomalous Electron Spin Lifetime in  $m\text{g}\text{b}_2$ . *Phys. Rev. Lett.* **101**, 177003 (2008).
- 27 Boross, P., Dóra, B., Kiss, A. & Simon, F. A unified theory of spin-relaxation due to spin-orbit coupling in metals and semiconductors. *Sci. Rep.* **3**, 3233 (2013).
- 28 Szolnoki, L., Dóra, B., Kiss, A., Fabian, J. & Simon, F. Intuitive approach to the unified theory of spin relaxation. *Phys. Rev. B* **96**, 245123 (2017).
- 29 Bernardi, M. First-principles dynamics of electrons and phonons. *Eur. Phys. J. B* **89**, 239 (2016).
- 30 Zhou, J.-J. *et al.* Perturbo: A software package for ab initio electron–phonon interactions, charge transport and ultrafast dynamics. *Comput. Phys. Commun.* **264**, 107970 (2021).
- 31 Zhou, J.-J. & Bernardi, M. Predicting charge transport in the presence of polarons: The beyond-quasiparticle regime in  $\text{SrTiO}_3$ . *Phys. Rev. Res.* **1**, 033138 (2019).
- 32 Li, W. Electrical transport limited by electron-phonon coupling from Boltzmann transport equation: An ab initio study of Si, Al, and  $\text{MoS}_2$ . *Phys. Rev. B* **92**, 075405 (2015).
- 33 Poncé, S., Margine, E. R. & Giustino, F. Towards predictive many-body calculations of phonon-limited carrier mobilities in semiconductors. *Phys. Rev. B* **97**, 121201 (2018).
- 34 Sohler, T. *et al.* Phonon-limited resistivity of graphene by first-principles calculations: Electron-phonon interactions, strain-induced gauge field, and Boltzmann equation. *Phys. Rev. B* **90**, 125414 (2014).
- 35 Lee, N.-E., Zhou, J.-J., Chen, H.-Y. & Bernardi, M. Ab initio electron-two-phonon scattering in GaAs from next-to-leading order perturbation theory. *Nat. Commun.* **11**, 1607 (2020).
- 36 Liu, T.-H., Zhou, J., Liao, B., Singh, D. J. & Chen, G. First-principles mode-by-mode analysis for electron-phonon scattering channels and mean free path spectra in GaAs. *Phys. Rev. B* **95**, 075206 (2017).
- 37 Ma, J., Nissimagoudar, A. S. & Li, W. First-principles study of electron and hole mobilities of Si and GaAs. *Phys. Rev. B* **97**, 045201 (2018).
- 38 Zhou, J.-J. *et al.* Ab Initio Electron-Phonon Interactions in Correlated Electron Systems. *Phys. Rev. Lett.* **127**, 126404 (2021).
- 39 Zhou, J.-J. & Bernardi, M. Ab initio electron mobility and polar phonon scattering in GaAs. *Phys. Rev. B* **94**, 201201(R) (2016).
- 40 Park, J., Zhou, J.-J. & Bernardi, M. Spin-phonon relaxation times in centrosymmetric materials from first principles. *Phys. Rev. B* **101**, 045202 (2020).
- 41 Kim, S., Woo, S. & Min, H. Vertex corrections to the dc conductivity in anisotropic multiband systems. *Phys. Rev. B* **99**, 165107 (2019).
- 42 Mahan, G. D. *Many-Particle Physics*. Physics of Solids and Liquids (Springer, 3rd ed., 2000).
- 43 Burkov, A. A. & Balents, L. Spin relaxation in a two-dimensional electron gas in a perpendicular magnetic field. *Phys. Rev. B* **69**, 245312 (2004).



- 44 Lépine, D. J. Spin Resonance of Localized and Delocalized Electrons in Phosphorus-Doped Silicon between 20 and 30 °K. *Phys. Rev. B* **2**, 2429–2439 (1970).
- 45 Lancaster, G., van Wyk, J. A. & Schneider, E. E. Spin-lattice relaxation of conduction electrons in silicon. *Proc. Phys. Soc.* **84**, 19–24 (1964).
- 46 Oertel, S., Hübner, J. & Oestreich, M. High temperature electron spin relaxation in bulk GaAs. *Appl. Phys. Lett.* **93**, 132112 (2008).
- 47 Kimel, A. V. *et al.* Room-temperature ultrafast carrier and spin dynamics in GaAs probed by the photoinduced magneto-optical Kerr effect. *Phys. Rev. B* **63**, 235201 (2001).
- 48 Bungay, A. R., Popov, S. V., Shatwell, I. R. & Zheludev, N. I. Direct measurement of carrier spin relaxation times in opaque solids using the specular inverse Faraday effect. *Phys. Lett. A* **234**, 379–383 (1997).
- 49 Dzhioev, R. I. *et al.* Suppression of Dyakonov-Perel Spin Relaxation in High-Mobility *n*-GaAs. *Phys. Rev. Lett.* **93**, 216402 (2004).
- 50 Lai, T. *et al.* Temperature dependence of electron-spin coherence in intrinsic bulk GaAs. *Appl. Phys. Lett.* **88**, 192106 (2006).
- 51 Ersfeld, M. *et al.* Unveiling Valley Lifetimes of Free Charge Carriers in Monolayer WSe<sub>2</sub>. *Nano Lett.* **20**, 3147–3154 (2020).
- 52 Li, J. *et al.* Valley relaxation of resident electrons and holes in a monolayer semiconductor: Dependence on carrier density and the role of substrate-induced disorder. *Phys. Rev. Mater.* **5**, 044001 (2021).
- 53 Yan, T., Yang, S., Li, D. & Cui, X. Long valley relaxation time of free carriers in monolayer WSe<sub>2</sub>. *Phys. Rev. B* **95**, 241406 (2017).
- 54 Goryca, M., Wilson, N. P., Dey, P., Xu, X. & Crooker, S. A. Detection of thermodynamic “valley noise” in monolayer semiconductors: Access to intrinsic valley relaxation time scales. *Sci. Adv.* **5**, eaau4899 (2019).
- 55 Hilton, D. J. & Tang, C. L. Optical Orientation and Femtosecond Relaxation of Spin-Polarized Holes in GaAs. *Phys. Rev. Lett.* **89**, 146601 (2002).
- 56 Krauß, M., Aeschlimann, M. & Schneider, H. C. Ultrafast Spin Dynamics Including Spin-Orbit Interaction in Semiconductors. *Phys. Rev. Lett.* **100**, 256601 (2008).